Research paper

Research on sand resistance performance of comprehensive protection facilities for desert hinterland highways under strong wind environment

Wenhua Yin[1], Xu Wang[2], Yongxiang Wu[3], Fang Wang[4]

Abstract: Based on the test and observation of the desert hinterland wind field, combined with the numerical simulation of Fluent wind-sand two-phase flow, the sand resistance performances of comprehensive protection in the desert hinterland under strong wind environment are researched. The transient wind speed and wind direction around the comprehensive protection facility are measured by two 3D ultrasonic anemometers on the highway in the desert hinterland, and the initial wind speed of the sand flow is provided for the numerical simulation boundary. The sedimentary sand particles around the comprehensive protection facility are collected for particle size analysis, and the particle size distributions of sedimentary sand particles at different locations are obtained. Numerical models of high vertical sand barriers, grass checkered sand barriers and roadbeds are established by Fluent, the wind-sand flow structures around the comprehensive protection facilities and desert hinterland highway under the strong wind environment are obtained, and the influence laws of the comprehensive protection facilities on the movement of wind-sand flow and sand deposition characteristics are obtained. The study found that the comprehensive protection facilities disturbed the wind and sand flow, and there are significant airflow partitions around the comprehensive protection facilities. The wind speed decreases rapidly after the wind-sand flows through the high vertical sand barrier; the wind-sand flow rises at the end of the high vertical sand barrier. When the wind-sand flow moves around the grass checkered sand barrier, the wind speed has dropped to the range of 0–3 m/s, and the wind speed near the ground by the grass checkered sand barrier is further reduced. Due to the existence of the concave surface of the grass grid, there are small vortices inside the grass grid sand barrier. Large sand particles are mainly deposited on the windward side and inside of high vertical sand barriers. The grass checkered sand barrier forms a stable concave surface to generate backflow, which can ensure that the sand surface does not sand itself in a strong wind environment, and can also make a small amount of sand carried in the airflow accumulate around the groove of the grass checkered sand barrier. The numerical simulation results are

[1]PhD., Lanzhou Jiaotong University, Civil Engineering College, Nanzhou, 353000, China; Ningxia Highway Survey and Design Institute Co., Ltd., China, e-mail: vonwa8111@126.com, ORCID: 0000-0001-9510-2373

[2]Prof., PhD., DSc., School of Civil Engineering, Lanzhou Jiaotong University, Lanzhou, 730070, China, e-mail: 2550702466@qq.com, ORCID: 0000-0001-5467-0382

[3]MSc., Eng., Ningxia Highway Survey and Design Insitute Co., Ltd, Yinchuan, 750001, China, e-mail: wuyongxiang2022@126.com, ORCID: 0000-0003-2675-3230

[4]MSc., Eng., Ningxia Highway Survey and Design Insitute Co., Ltd, Yinchuan, 750001, China, e-mail: fangwang0531@163.com, ORCID: 0000-0002-8088-7697

consistent with the measured results, and the comprehensive protection measures have achieved good sand control effects.

1. Introduction

There are large desert areas in the northwest of China. The movement of wind sand flow is active. The extreme wind speed is as high as 30 m/s, and the infrastructure is severely damaged by wind sand flow. With the rapid construction of highways in China, more new highways will pass through desert areas, and the safety of highway operations will be seriously threatened by wind sand flow. Many scholars have carried out in-depth research on the movement and protection of sand flow [1–6]. The comprehensive sand protection facility composed of two or more kinds of sand protection facilities has better sand protection performance and is gradually widely used along the desert hinterland highway [6–10].

The existing wind sand flow protection facilities mainly include high vertical sand barriers, various types of sand retaining walls, grass checkered sand barriers and sand plant protection [11–15]. Lima al. [16] studied the variation of wind speed around the porous fence, and did detailed research on parameters such as porosity and hole spacing of the fence, and obtained the wind shear velocity near the surface. Marko et al. [17] studied the ground shear stress field around the railway subgrade and the track, and analyzed the erosion and deposition rules of the wind-sand flow around the railway track. Zhang et al. [18] studied the wind-proof and sand-fixing effect of HDPE board sand barriers, and used wind-proof efficiency and sand-control efficiency to evaluate the protection effect of sand barriers on infrastructure. The research shows that when the porosity is 30%, the wind and sand prevention effects of single row are 46% and 65.3%, respectively. The first row of sand control fences in the multi-row protection plays a major protective role. Wang et al. [19] studied the protective effects of two sand barriers with perforated plates and steel meshes with a porosity of 48% in a wind tunnel. The experimental results show that the perforated plate fence reduces the wind speed more than the wire mesh fence. Bo et al. [20] studied the influence law of the grass checkered sand barrier on the wind speed, and the study showed that when the airflow passes through the grass checkered sand barrier, the spatial variation of its velocity can be divided into three stages: decline, stabilization and recovery. The variation of wind velocity with height satisfies three different logarithmic linear functions.

This paper aims at the comprehensive protection facilities formed by the combination of high vertical sand barriers and grass checkered sand barriers. Based on the wind field test in the desert hinterland and the numerical simulation of Fluent Euler two-phase flow, the comprehensive protection facilities and the wind-sand flow structure around the desert hinter road in the strong wind environment are studied. The influence law of comprehensive protection facilities on sand flow movement and sand deposition characteristics is gained, in order to provide a reference for the prevention and control of sand flow catastrophe in desert hinterland roads under strong wind environment.

2. On-site testing of comprehensive protective facilities

2.1. Field tested scheme

Figure 1 shows the comprehensive protection facilities for the highway in the hinterland of the Tengger Desert in Zhongwei City, Ningxia Province, including 4 rows of high vertical sand barriers with an interval of 6 m and 25 rows of grass checkered sand barriers with an interval of 1 m. Fig. 2 shows the layout of the field measurement in the desert hinterland. A total of two Gill Wind Master Pro three-dimensional ultrasonic anemometers are arranged, and the sampling and output frequencies are both 32 Hz. The 1# measuring point is located 1m in front of the windward side of the first row of sand barriers and at a height of 1m from the ground, and the 2# measurement point is located 1m behind the leeward side of the fourth row of sand barriers and at a height of 1m from the ground. Long-term wind speed
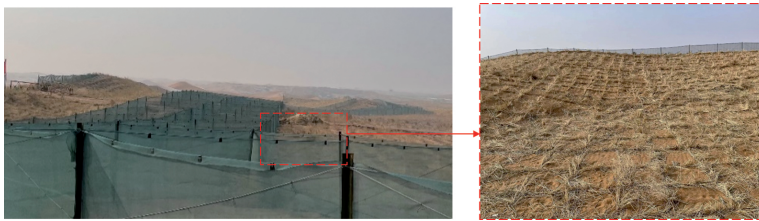

Fig. 1. Map of comprehensive protection facilities for highways in the desert hinterland
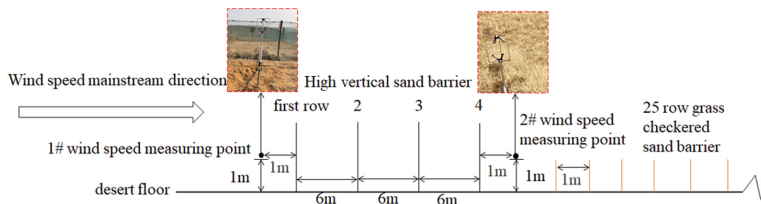

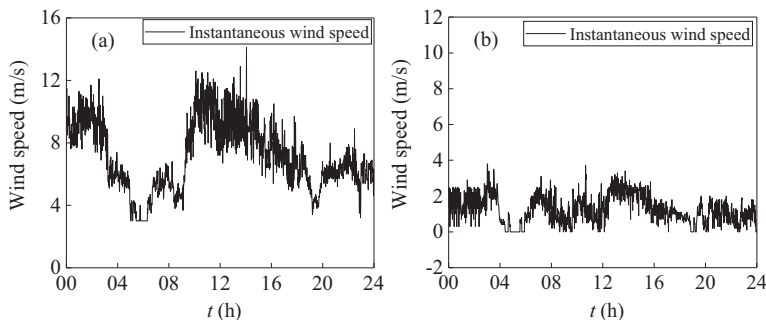Fig. 2. Layout map of field measurement in desert hinterland

Fig. 3. Time-history data diagram of strong wind period: (a) Windward side; (b) Leeward side

sampling will start at 00:00 on March 7, 2022. Fig. 3 shows the time-history data of wind speed captured on a windy day on March 17, 2022. The rose diagram of wind direction is obtained as shown in Fig. 4. The characteristics of sand and dust deposition around the high vertical sand barriers and grass checkered sand barriers are shown in Fig. 5.
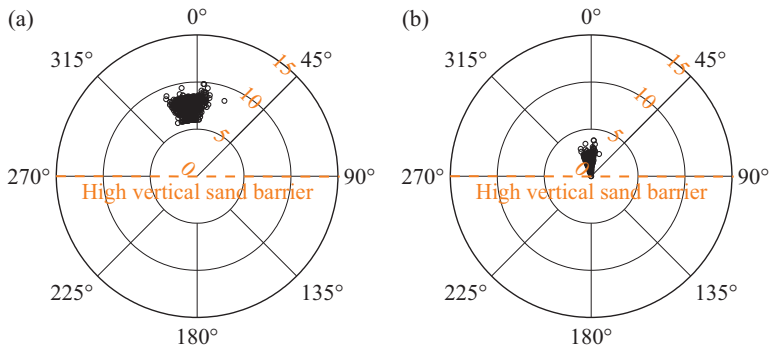

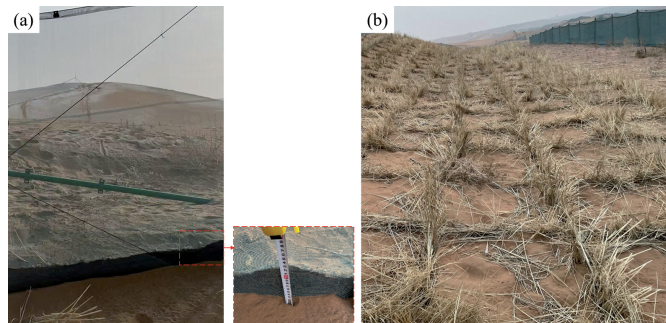Fig. 4. Wind rose diagram: (a) Windward side; (b) Leeward side

Fig. 5. Sand deposition characteristics: (a) High vertical sand barrier;
(b) Grass checkered sand barrier

2.2. Analysis of field test results

It can be seen from the wind rose diagram that the mainstream wind direction is within 350°–10°, which proves that the high vertical sand barriers are arranged perpendicular to the mainstream direction. The initial wind speed of sand particles obtained from the preliminary experiments and guidance in the desert road design document was 5.2 m/s, and the statistics of wind speed data greater than 5.2 m/s showed that the average wind speed was 10.12 m/s, the maximum wind speed was 14 m/s, and more than half of the day was in the strong wind period. The front high vertical sand barrier quickly reduces the wind speed at a height of 2 m near the ground, and the wind speed on the leeward side of the four rows of sand barriers is lower than 5 m/s. Sand particles are first deposited on the windward

side and inside of the first row of high vertical sand barriers. The sand particles around the high vertical sand barriers and the grass checkered sand barriers were brought back to the laboratory for particle size analysis. The small-diameter sand and dust with a diameter ranging from 0.063 mm to 0.125 mm passed through the high vertical sand barrier with the airflow and deposited inside the high vertical sand barrier or continued to move toward the grass checkered sand barrier [21]. The grass checkered sand barrier reduces the speed of wind and sand flow within 0.2m above the ground again, and a concave surface is formed near the ground, which further restricts the movement of sand particles, and it is difficult for small particles of sand to jump again.

3. Two-phase flow model of wind and sand

3.1. Geometric Modeling and Meshing

The 2D geometric model of the 1:1 grass checkered sand barrier and the roadbed is established by ICEM CFD software as shown in Fig. 6 – 25, 50, 75, and 100 rows are set up at intervals of 1m, respectively. The two-dimensional geometric model of the comprehensive protection facility composed of high vertical sand barriers and grass checkered sand barriers is shown in Fig. 7. The height of the high vertical sand barrier is 1.7 m, and 4 rows are arranged at an interval of 6 m; the height of the grass grid is 0.2 m, and 25 rows are arranged at an interval of 1 m. The monolithic subgrade (two-way four-lane) is used with a pavement width of 26 m, a subgrade height of 2.5 m, a slope ratio of 1:4, a height of the computational domain of 30 m, and a total length of 196 m. The combination of unstructured and structured grid is adopted, the high vertical sand barrier adopts structured grid, and the rest adopts unstructured grid. The overall mesh size ranges from 1 to 10 mm, and the quality of the mesh is qualified. The total number of model meshes is about 3 million. The meshes and boundary conditions of the comprehensive protection facility and
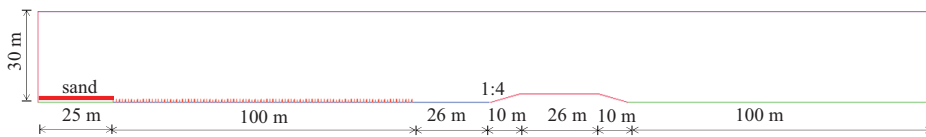

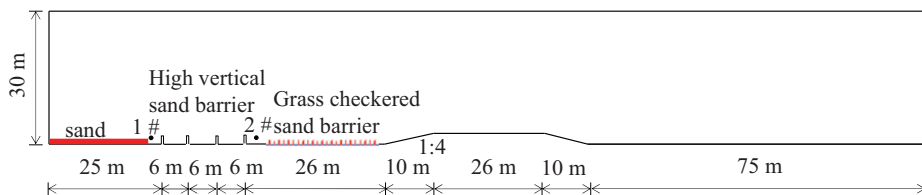Fig. 6. Grass checkered sand barrier and subgrade geometry models

Fig. 7. Integrated protective facilities and subgrade geometric models

roadbed are shown in Fig. 8. The boundary condition settings for the grass checkered sand barrier model are the same.
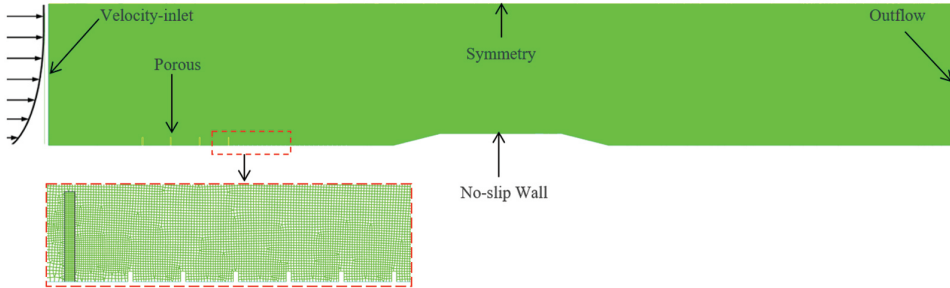

Fig. 8. Sand Barrier and Subgrade Mesh and Boundary Conditions

3.2. Boundary conditions and calculation parameters

Velocity-inlet is used for the left boundary. The measured wind speed is close to 10 m/s. Taking 10 m/s as the speed of the wind-sand flow in the numerical model can simulate the movement of the wind-sand flow more realistically. Equation (3.1) is used to generate the wind speed profile. The right boundary is taken as the outlet boundary. The top adopts symmetry. No-slip Wall is used for the ground and subgrade, and the rough height is 0.02 m. Both the high vertical sand barrier and the grass checkered sand barrier are simulated by porous media, and the ventilation rates are 0.5 and 0.3, respectively [20]. A 0.15 m high and 20 m long area of sand bed is set up in front of the sand barrier, and the sand particle size in the sand flow is 0.1 mm.

$$(3.1) \qquad v(y) = \left(\frac{v^*}{k}\right) \ln\left(\frac{y}{z_0}\right)$$

where: v^* is the friction wind speed, k is the von Karman constant, usually taken as 0.4, z_0 is rough height.

3.3. Theory of two-phase flow of wind and sand

The airflow velocity studied in this paper $v < 50$ m/s, can be considered an incompressible fluid and the effects of gravity are taken into account [22].

Establish the continuity equation (3.2)

$$(3.2) \qquad \frac{\partial(\varphi_r \rho_r)}{\partial t} + \frac{\partial(\varphi_r \rho_r u_x)}{\partial t} + \frac{\partial(\varphi_r \rho_r u_y)}{\partial t} = 0$$

where: u_x and u_y are components of velocity in the x and y directions, respectively; φ_r and ρ_r are the volume fraction and density of the rth phase.

Establish the momentum equation (3.3) as

(3.3)
$$\frac{\partial}{\partial t}(\varphi_g \rho_g U_g) + \nabla(\varphi_g \rho_g U_g U_g) = -\varphi_g \nabla p + \nabla \tau_g + \varphi_g \rho_g g + f_{sg}$$

$$\frac{\partial}{\partial t}(\varphi_s \rho_s U_s) + \nabla(\varphi_s \rho_s U_s U_s) = -\varphi_s \nabla p - \nabla p_s + \nabla \tau_s + \varphi_s \rho_s g + f_{sg}$$

where: φ_g and ρ_g are the gas phase volume fraction and density, φ_s and ρ_s are the solid phase volume fraction and density, $\varphi_s + \varphi_g = 1$; and f_{sg} is the force between the gas phase and the solid phase; U_g and U_s are gas phase and solid phase velocity, respectively; p for shared pressure; p_s is the solid phase pressure; g is the acceleration of gravity.

3.4. Theory of Porous Media

Adding a momentum source term to the momentum equation (3.4) can mold the action of a porous medium. The source term consists of two parts, the tack loss term and the inertia loss term [22].

(3.4)
$$S_i = -\left(\sum_{j=1}^{3} D_{ij} u v_j + \sum_{j=1}^{3} C_{ij} \frac{1}{2} \rho |v| v_j\right)$$

where: S_i is the source term of the momentum equation, $|v|$ is the velocity magnitude, and D and C are the matrices. The momentum source term has an effect on the pressure gradient of the porous media region, and for isotropic porous media, the momentum source term can be expressed equation (3.5) as:

(3.5)
$$S_i = -\left(\frac{u}{\alpha} v_j + C_2 \frac{1}{2} \rho |v| v_j\right)$$

where: α is the permeability coefficient and C_2 is the inertial resistance coefficient, that is, the D and C matrices are reduced to diagonal matrices, the coefficients on the diagonal are α and C_2, and the other elements are 0.

3.5. Grid Independence Verification

To verify the mesh independence of the CFD numerical model, the grid size parameters of the comprehensive protection facilities and the roadbed are adjusted to establish a grid model with three resolution levels of low, medium and high resolution levels of 2 million, 3 million, and 4 million grid cells respectively. A wind speed of 10 m/s was applied at the velocity inlet, and the wind velocity profile was monitored 5 m behind the velocity inlet and 1 m behind the leeward side of the high vertical sand barrier. Fig. 9 shows the comparison of the three model monitoring indicators. The results show that the model with 3 million grid cells is in good agreement with the model with 4 million cells, and the relative error only differs by about 3%. For 2 million grids, the wind speed results on the leeward side of the sand barrier have a large deviation. A model with a number of 3 million grid cells is reasonably accurate.
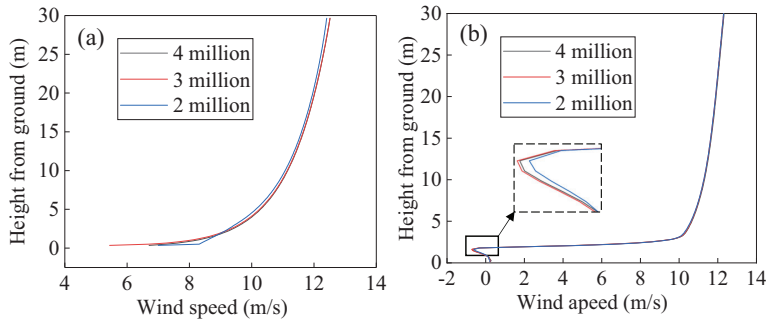
Fig. 9. Comparison of wind speed profiles under different grid resolutions: (a) 5 m behind the entrance, (b) 1 m behind the leeward side of the high vertical sand barrier

4. Analysis of numerical results

4.1. Analysis on windproof performance of comprehensive protection facilities

Based on-site measurements, the average wind speed in the desert hinterland reaches 10.12 m/s, so the speed of wind and sand flow is 10 m/s. The dominant wind direction is from left to right, and the sand barriers around the protection facility and the wind-sand flow structure around the roadbed are simulated. Fig. 10 is the wind speed cloud map around the sand barrier with a subgrade height of 2.5 m, a slope of 1:4, and 25 rows of grass lattices. Fig. 11 shows the wind speed cloud map around the subgrade height of 2.5 m, slope of 1:4; 4 rows of 1.7 m high vertical sand barriers and 25 rows of grass checkered sand barriers.

Fig. 10. Cloud map of wind speed around the grass checkered sand barrier

The following findings are obtained from Figs. 10 and 11 that the protective facility disturbs the wind-sand flow, and there is a significant airflow partition around the protective facility. There is only a grass checkered sand barrier, and the wind speed inside the grass checkered sand barrier 0.2 m near the ground is in the low wind speed area (wind speed less than 2.4 m/s), 0.5 m above the grass checkered sand barrier is in a laminar flow state, and the wind speed changes rapidly at 3.6–10.8 m/s. The comprehensive protection facilities
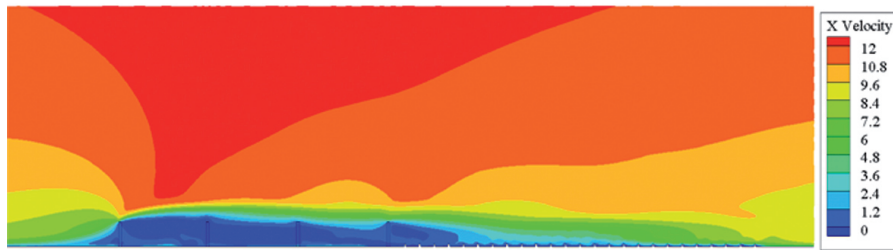
Fig. 11. Cloud map of wind speed around comprehensive protection facilities

block the wind and sand flow, and the wind speed decreases rapidly, and a deceleration area appears on the windward side of the first row of high vertical sand barriers, and the wind speed drops below 6 m/s. After the airflow passes through the high vertical sand barrier, the leeward side of the sand barrier forms a low wind speed area. The airflow above the first row of high vertical sand barriers is lifted, forming a high wind speed area above the second and third rows of high vertical sand barriers. Due to the reduction of the wind speed by the four rows of high vertical sand barriers, the 2 m above the grass checkered sand barrier is also in the low wind speed area, and the wind speed around the grass checkered sand barrier is further reduced.

In order to further analyze the wind speed near the ground, extract the wind speed along the way at 0.15 m, 0.20 m and 0.50 m from the ground for the grass grid and the roadbed model, as shown in Fig. 12. The wind speeds of 0.15 m, 0.5 m, 1.0 m, 1.5 m, and 2.0 m along the way near the ground are extracted from the comprehensive protection facilities and the roadbed model, as shown in Fig. 13. The wind speed changes most drastically at 0.5 m. In order to better compare and analyze the windproof effect of the protective facilities, the wind speeds along the route are extracted for three working conditions: no protection on the ground, grass grid protection and comprehensive protection. Fig. 14. Table 1 shows the speed changes around the subgrade under three working conditions with a height of 0.5 m.

The grass checkered sand barrier can quickly reduce the wind speed of 0.2 m near the ground. At the ground height of 0.5 m, the airflow speed and wind speed do not decrease significantly. The comprehensive protection facilities can decelerate the airflow within 2 m of the ground. The airflow is quickly blocked around the high vertical sand barrier, and the horizontal wind speed is reduced to a minimum of about 5 m/s. The airflow above 1.7 m is lifted above the high vertical sand barrier. The internal wind speed of the high vertical sand barrier is reduced to about 2.5 m/s, the wind speed direction is complex and changeable, and the vertical wind speed fluctuates positively and negatively in the range of $-2 \div 2$ m/s. After the airflow passes through the high vertical sand barrier, the horizontal wind speed around the grass square sand barrier is reduced to 0–3 m/s; the grass square increased the roughness of the ground, and the wind speed near the ground is further reduced. The comprehensive protection facilities can reduce the wind speed around the highway in the desert hinterland, and the wind speed at the foot of the windward slope is reduced to 0.3 m/s, with a reduction rate of 95.38%, while the grass checkered sand barrier
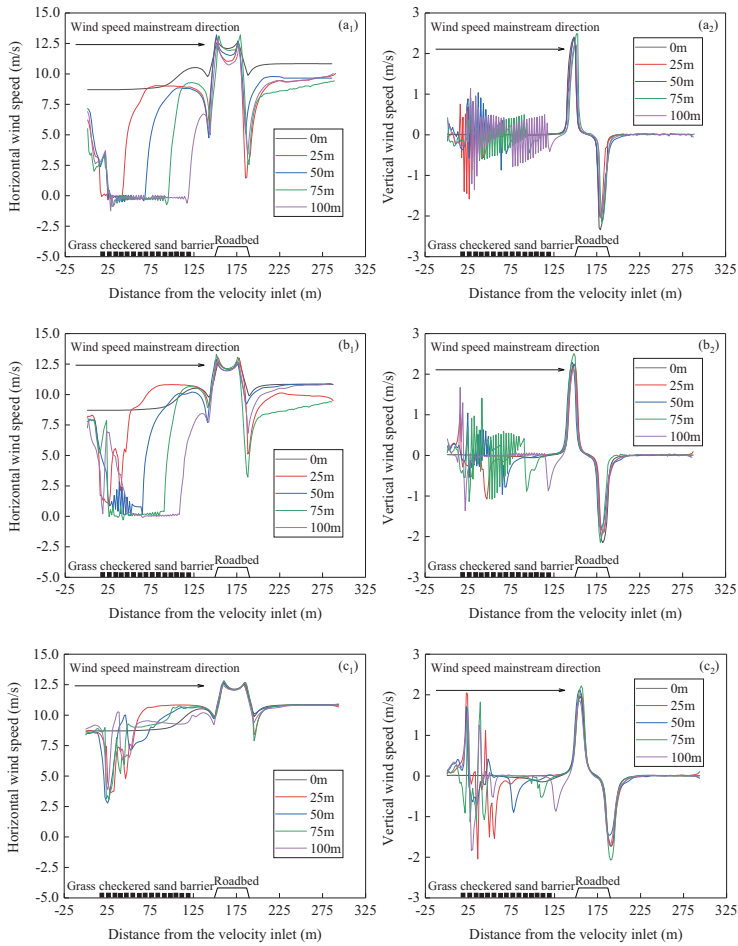
Fig. 12. Distribution map of wind speed along the grass checkered sand barrier and roadbed:
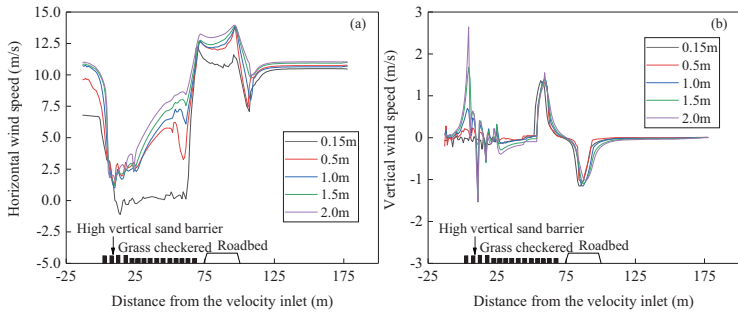(a) 0.15 m above ground; (b) 0.20 m above ground; (c) 0.50 m above ground

Fig. 13. Distribution map of wind speed along the way at different heights of comprehensive protection
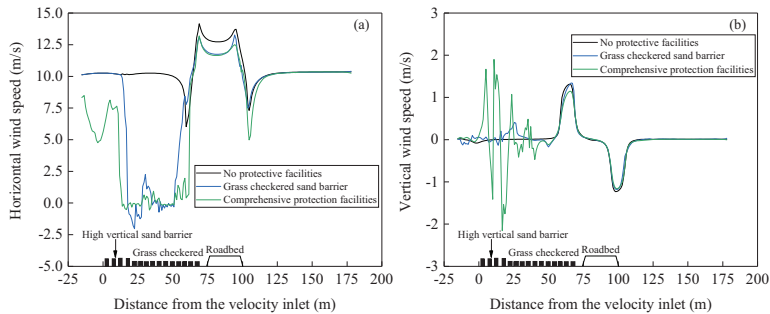facilities:(a) Horizontal wind speed; (b) Vertical wind speed

Fig. 14. Distribution of wind speed at 0.5 m height: (a) Horizontal wind speed;
(b) Vertical wind speed

Table 1. Variation of horizontal velocity at a height of 0.5 m above the ground under different
protections

Position	No sand barrier protection	Grass checkered sand barrier protection		Comprehensive facility protection	
	Wind speed value (m/s)	Wind speed value (m/s)	Decrease rate (%)	Wind speed value (m/s)	Decrease rate (%)
Leeward side of high vertical sand barrier	10.0	10.0	0.0	−2.0	120.0
Leeward side of grass checkered sand barrier	10.0	−1.60	116.0	−0.4	104.0
Windward slope foot	6.50	1.50	76.92	0.3	95.38
Windward Slope Shoulder	14.5	13.3	8.28	12.8	11.72
Leeward slope foot	7.60	7.50	1.32	5.40	28.95
Leeward Slope Shoulder	13.8	13.2	88.41	12.4	10.14

has no obvious effect. Therefore, the comprehensive protection facilities composed of high
vertical sand barriers and grass checkered sand barriers reduce the near-surface wind speed
in all directions, and delay the movement rate of wind-sand flow.

4.2. Sand deposition characteristics

Figures 15–17 are the cloud map of the sand volume fraction around the grass checkered sand barrier and the comprehensive protection facility. The wind direction is from left to right, and different colors represent different volume fractions (blue is the smallest, red is the largest).

This is shown in Fig. 15 – when only the grass checkered sand barrier is set up for protection, the sand particles first accumulate in front of the first row of grass checkered sand barriers. Because the grass checkered sand barrier has a poor effect on wind speed reduction, and the sand grains have strong movement ability, the a grains jump to the rear grass checkered sand barrier and settle after being carried by the airflow. There is a recirculation zone inside the grass checkered sand barrier, and part of the sedimentary sand particles will move to the leeward side of the grass checkered sand barrier with the vortex movement and accumulate again. Therefore, there are relatively few sand particles in the center of the grass square, and the sand particles are piled up inside the grass square sand barrier to form a concave surface, which is consistent with the field observation results. With the increase of the number of grass squares, the movement rate of wind sand flow gradually decreases. If conditions permit, more grass checkered sand barriers can be set up to increase surface roughness and reduce the speed of sand movement.
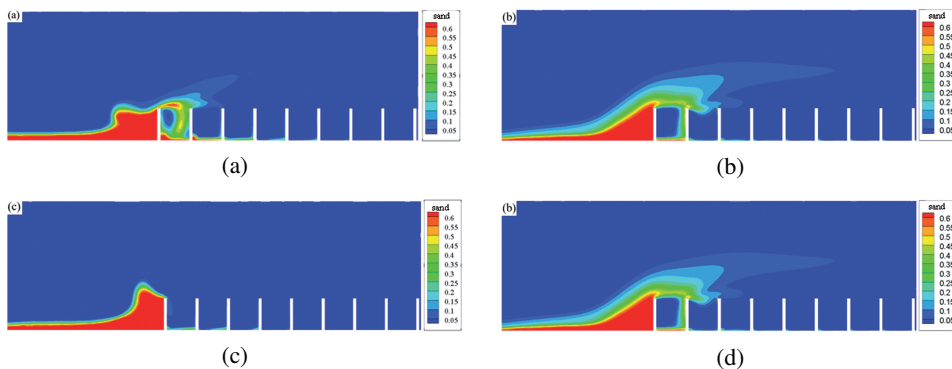

(a)

(b)

(c)

(d)

Fig. 15. Cloud map of the volume fraction of sand around the grass checkered sand barrier: (a) 25 sand barriers (b) 50 sand barriers (c) 75 sand barriers (d) 100 sand barriers

The following findings are obtained from Fig. 16 that when the sand is protected by the high vertical sand barriers, the sand movement around the first row of high vertical sand barriers is active, and most of the large particles of sand and dust are deposited on the windward side of the sand barriers. After passing through the first row of high vertical sand barriers, small particles of sand are mainly deposited inside the first and second rows of high vertical sand barriers due to the sharp drop in wind speed. The high vertical sand barrier has good wind resistance, and the large sand particles are basically intercepted inside the high vertical sand barrier, and some small sand particles continue to move or deposit over the high vertical sand barrier. The high vertical sand barrier delays the movement of wind

and sand flow, so that the sand particles of 2 m near the ground are deposited around the sand barrier.
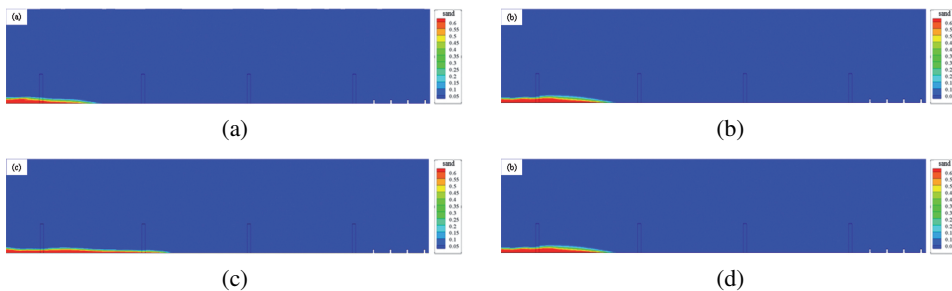

Fig. 16. Cloud map of the volume fraction of sand particles around the high vertical sand barrier of the comprehensive protection facility: (a) $t = 1$ s, (b) $t = 2$ s, (c) $t = 3$ s, (d) $t = 4$ s, (e) $t = 5$ s, (f) $t = 6$ s, (g) $t = 7$ s

The following findings are obtained from Fig. 17 that when the high vertical sand barriers and grass checkered sand barriers are set up, the air flow passes through the four rows of high vertical sand barriers, and the wind speed has been reduced rapidly. In the near-ground area, the ventilation rate of the grass checkered sand barrier is lower, and the grass checkered sand barrier increases the surface roughness. Most of the sand that passes through the high vertical sand barrier is deposited in the interior of the grass square, and gradually accumulates with the increase of sand. The mechanism is: the grass square forms a stable concave surface, which produces a backflow in the groove, which has a lift effect on the airflow at the top, that is, the "lift effect". It can ensure that the sand surface does not have sand by itself in a strong wind environment, and can also make a small amount of sand particles carried in the airflow accumulate around the grooves of the grass squares. Therefore, the high vertical sand barrier and the grass square sand barrier can reduce the wind speed and slow down the movement rate of the wind and sand flow in a larger range, and the grass square can fix the sand and gradually accumulate around it until it is buried. The comprehensive sand control facilities in the desert hinterland have achieved good sand control and sand fixation effects.

5. Conclusions

(1) The high vertical sand barriers are mainly arranged perpendicular to the mainstream wind direction. The average wind speed is 10.12 m/s and the maximum wind speed is 14 m/s during the strong wind period. The front high vertical sand barrier quickly reduces the wind speed at a height of 2 m near the ground, and the large-diameter sand and dust with a diameter greater than 0.125 mm is deposited around the high vertical sand barrier, and the measured sand and dust deposition thickness is up to 12.1 cm. The small-diameter sand and dust with a diameter ranging from 0.063 mm to 0.125 mm passed through the
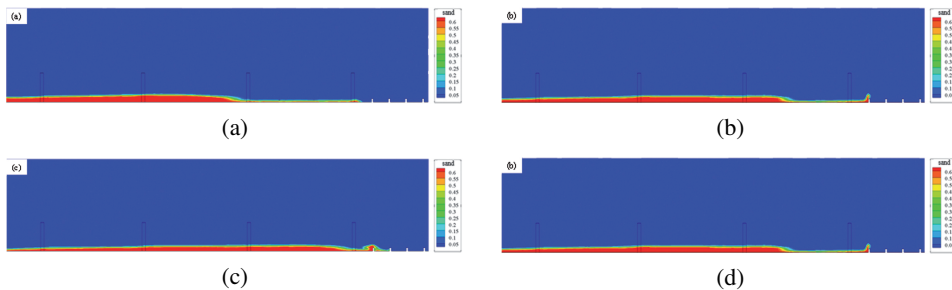
Fig. 17. Cloud map of the volume fraction of sand in the grass checkered sand barrier of the comprehensive protection facility: (a) $t = 8$ s, (b) $t = 9$ s, (c) $t = 10$ s, (d) $t = 11$ s, (e) $t = 12$ s

high vertical sand barrier with the airflow, and finally deposited on the grass checkered sand barrier, which was difficult to jump again.

(2) Comprehensive protection facilities reduce the wind speed near the ground in all directions. The comprehensive protection facilities disturbed the wind and sand flow, and there were significant airflow partitions around the comprehensive protection facilities. The wind and sand flow at a height of 1.7 m above the ground quickly decreased after passing through the first row of high vertical sand barriers. Wind sand flow above 1.7 m rises at the end of the high vertical sand barrier. When the wind-sand flow moves around the grass checkered sand barrier, the wind speed has dropped to the range of 0–3 m/s, and there are small vortices inside the grass checkered sand barrier. The grass square increases the roughness of the ground, and further reduces the wind speed near the ground.

(3) Compared with a single protective structure, the sand control effect of comprehensive protective measures is better. The wind speed around the high vertical sand barrier decreases, the energy of the airflow carrying the sand particles decreases, and the large sand particles are mainly deposited on the windward side and the interior of the high vertical sand barrier. The grass square forms a stable concave surface to generate backflow, which can ensure that the sand surface does not produce sand by itself in a strong wind environment, and can also allow a small amount of sand particles carried in the airflow to accumulate around the grooves of the grass square. The numerical simulation results are consistent with the measured results.

Acknowledgements

References

[1] Z.S. An, K.C. Zhang, L.H. Tan, et al., "Dune dynamics in the southern edge of Dunhuang Oasis and implications for the oasis protection", *Journal of Mountain Science*, 2018, vol. 15, no. 10, pp. 2172–2181; DOI: 10.1007/s11629-017-4723-2.

[2] Z.T. Wang, Z.S. An, "A simple theoretical approach to the thermal expansion mechanism of salt weathering", *Catena*, 2016, vol. 147, pp. 695–698; DOI: 10.1016/j.catena.2016.08.033.

[3] K.C. Zhang, Z.S. An, D.W. Cai, et al., "Key Role of Desert-Oasis Transitional Area in Avoiding Oasis Land Degradation from Aeolian Desertification in Dunhuang, Northwest China", *Land Degrandation Development*, 2017, vol. 28, no. 1, pp. 142–150; DOI: 10.1002/ldr.2584.

[4] W.C. Yang, H. Yue, E. Deng, "Research on wind and sand resistance performance of high vertical sand barriers in desert hinterland highways", *Journal of Railway Science and Engineering*, 2022, pp. 1–11; DOI: 10.19713/j.cnki.43-1423/u.T20220250.

[5] L. Shi, D.Y. Wang, K.C. Li, "Windblown sand characteristics and hazard control measures for the Lanzhou–Wulumuqi high-speed railway", *Natural Hazards*, 2020, vol. 104, pp. 353–374; DOI: 10.1007/s11069-020-04172-9.

[6] T.L. Bo, X.J. Zheng, S.Z. Duan, et al., "The influence of wind velocity and sand grain diameter on the falling velocities of sand particles", *Powder Technology*, 2013, vol. 241, pp. 158–165; DOI: 10.1016/j.powtec.2013.02.043.

[7] S.B. Xie, J.J. Qu, Y.J. Pang, "Dynamic wind differences in the formation of sand hazards at highand low-altitude railway sections", *Journal of Wind Engineering & Industrial Aerodynamics*, 2017, vol. 169, pp. 39–46; DOI: 10.1016/j.jweia.2017.07.003.

[8] Y. Tominaga, T. Okaze, A. Mochida, "Wind tunnel experiment and CFD analysis of sand erosion/deposition due to wind around an obstacle", *Journal of Wind Engineering & Industrial Aerodynamics*, 2018, vol. 182, pp. 262–271; DOI: 10.1016/j.jweia.2018.09.008.

[9] W.H. Sun, N. Huang, "Influence of slope gradient on the behavior of saltating sand particles in a wind tunnel", *Catena*, 2017, vol. 148, pp. 145–152; DOI: 10.1016/j.catena.2016.07.013.

[10] Y.H. Hao, Y.J. Feng, J.C. Fan, "Experimental study into erosion damage mechanism of concrete materials in a wind-blown sand environment", *Construction and Building Materials*, 2016, vol. 111, pp. 662–670; DOI: 10.1016/j.conbuildmat.2016.02.137.

[11] K.C. Zhang, J.J. Qu, K.T. Liao, et al., "Damage by wind-blown sand and its control along Qinghai-Tibet Railway in China", *Aeolian Research*, 2010, vol. 1, no. 3-4, pp. 143–146; DOI: 10.1016/j.aeolia.2009.10.001.

[12] Y. Zhang, Y. Wang, P. Jia, "Investigation of the statistical features of sand creep motion with wind tunnel experiment", *Aeolian Research*, 2014, vol. 12, pp. 1–7; DOI: 10.1016/j.aeolia.2013.10.007.

[13] N. Bar, T. Elperin, I. Katra, et al., "Numerical study of shear stress distribution at sand ripple surface in wind tunnel ?ow", *Aeolian Research*, 2016, vol. 21, pp. 125–130; DOI: 10.1016/j.aeolia.2016.04.007.

[14] N. Xiao, Z.B. Dong, S. Xiao, et al., "An improved approach to estimate sand-driving winds", *Journal of Cleaner Production*, 2021, vol. 285, art. ID 124820; DOI: 10.1016/j.jclepro.2020.124820.

[15] H.Z. Yizhaq, Z.W. Xu, Y. Ashkenazy, "The effect of wind speed averaging time on the calculation of sand drift potential: New scaling laws", *Earth and Planetary Science Letters*, 2020, vol. 544, art. ID 116373; DOI: 10.1016/j.epsl.2020.116373.

[16] I.A. Lima, E.J.R. Parteli, Y.P. Shao, et al., "CFD simulation of the wind ?eld over a terrain with sand fences: Critical spacing for the wind shear velocity", *Aeolian Research*, 2020, vol. 43, art. ID 100574; DOI: 10.1016/j.aeolia.2020.100574.

[17] M. Horvat, L. Bruno, S. Khris, "CWE study of wind ?ow around railways: Effects of embankment and track system on sand sedimentation", *Journal of Wind Engineering & Industrial Aerodynamics*, 2021, vol. 208, art. ID 104476; DOI: 10.1016/j.jweia.2020.104476.

[18] K. Zhang, P.W. Zhao, J.C. Zhao, et al., "Protective effect of multi-row HDPE board sand fences: A wind tunnel study", *International Soil and Water Conservation Research*, 2021, vol. 9, no. 1, pp. 103–115; DOI: 10.1016/j.iswcr.2020.08.006.

[19] T. Wang, J.J. Qu, Y.Q. Ling, et al., "Shelter effect efficacy of sand fences: A comparison of systems in a wind tunnel", *Aeolian Research*, 2018, vol. 30, pp. 32–40; DOI: 10.1016/j.aeolia.2017.11.004.

[20] T.L. Bo, P. Ma, X.J. Zheng, "Numerical study on the effect of semi-buried straw checkerboard sand barriers belt on the wind speed", *Aeolian Research*, 2015, vol. 16, pp. 101–107; DOI: 10.1016/j.aeolia.2014.10.002.

[21] L. Opyrchał, R. Chmielewski, A. Bąk, "New method for comparing of particle-size distribution curve", *Archives of Civil Engineering*, 2022, vol. 68, no. 1, pp. 63–72; DOI: 10.24425/ace.2022.140156.

[22] X.X. Wu, Z.Y. Guo, R.D. Wang, et al., "Optimal design for wind fence based on 3D numerical simulation", *Agricultural and Forest Meteorology*, 2022, vol. 323, art. ID 109072; DOI: 10.1016/j.agrformet. 2022.109072.